Acta Astronautica 105 (2014) 373–384

Contents lists available at ScienceDirect

Acta Astronautica

journal homepage: www.elsevier.com/locate/actaastro

Tethered towing using open-loop input-shaping and discrete thrust levels

Lee Jasper*, Hanspeter Schaub

Aerospace Engineering Sciences Department, ECNT 321, 431 UCB Colorado Center for Astrodynamics Research, University of Colorado, Boulder, CO 80309-0431, USA

ARTICLE INFO

Article history:
Received 23 April 2014
Received in revised form
14 September 2014
Accepted 2 October 2014
Available online 13 October 2014

Keywords:
Space debris
Active debris removal
Tether
Input shaping
Bang-off-bang
Posicast

ABSTRACT

Asteroid retrieval, satellite servicing, and debris removal concepts often rely on a thrusting vehicle to redirect and steer a passive object. One effective way to tow the object is through a tether. This study employs a discretized tether model attached to six degree-of-freedom end bodies. To reduce the risk of a post-burn collision between the end bodies, discrete thrust input shaping profiles are considered including a Posicast input and a bang-off-bang thrust profile. These input shaping techniques attain desirable collision avoidance performance by inducing a tumbling or gravity gradient motion of the tethered formation. Their performance is compared to an earlier frequency notched thruster profile.

1. Introduction

The concept of towing objects in space has been gaining interest because it is useful for a variety of mission concepts. NASA has proposed several missions to asteroids to study them while developing deep-space exploration techniques (NASA FY2014 Complete Budget[1]). However, NASA also wants to retrieve an asteroid and return it to a near Earth orbit for easier access [1]. There are several ideas for capturing the asteroid; however, the process of imparting Δv to the object has received less attention. Towing also has been proposed for satellite servicing as well as Active space Debris Removal (ADR) [2]. The beneficial effects of reducing debris growth by using ADR are being actively investigated [3–5]. Another active research avenue for ADR is the many challenging questions about the process of attaching a tether to the debris object [2,6–8]. However, there are fewer studies of what thruster burns to perform to change the debris' orbit while maintaining a low collision risk. Recently, there has been expanding interest in towing with a tether for ADR. These studies show that using a step input thrust profile (full thrust on, all thrust off once Δv achieved) produces challenging end body dynamics [9–12] and wrap up concerns [13]. This paper addresses the dynamics and open-loop thrusting control of towing large end bodies in space while considering both continuous and discrete/impulsive thrusting profiles to avoid many of these undesirable behaviors.

The tethered-tug concept discussed here focuses on space debris objects. However, the basic concept is applicable to small asteroid and satellite towing mission concepts as well. Fig. 1 demonstrates the towing mission concept where a craft, capable of actively thrusting (referred to as the 'tug'), is tethered to the passive object: debris, asteroid, or satellite to be serviced.

When specifically considering the ADR mission, Fig. 1(a), the tug could be a rocket that is assumed to have deployed its

* Corresponding author.
E-mail addresses: Lee.Jasper@colorado.edu (L. Jasper), Hanspeter.Schaub@colorado.edu (H. Schaub).
URL: http://hanspeterschaub.info (H. Schaub).
[1] http://www.nasa.gov/news/budget/index.html

http://dx.doi.org/10.1016/j.actaastro.2014.10.001
0094-5765/

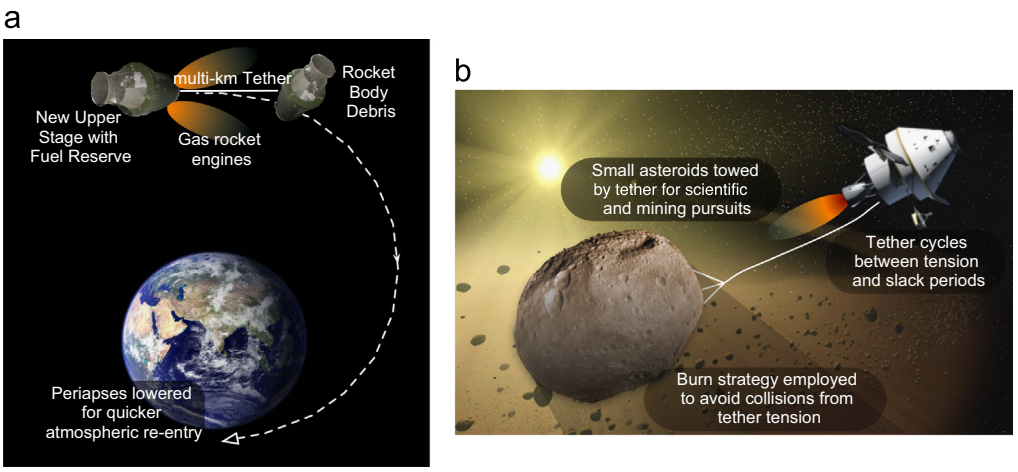

Fig. 1. Examples of tethered tug concepts. (a) Tethered ADR concept with rocket bodies. (b) Tethered tug with a small asteroid.

payload and completed its primary mission. Its secondary mission goal is to use the remaining fuel reserves to rendezvous with a debris object with similar orbital parameters. While it may be optimistic to think that the ADR mission is a secondary goal [14], it is likely possible to modify upper stages to perform an ADR mission. Previous rendezvous and proximity operation missions that demonstrate many relevant technologies to ADR are summarized in Reference [15]. After attaching a tether to the debris, the tug engages a single large thrust burn thus lowering the periapsis of both objects. The increased drag forces cause both objects to deorbit within 25 years. Depending upon initial starting altitude and amount of reserve fuel available to the active upper stage, the debris–tug system could be deorbited within half an orbit [11,16,17], but it is assumed for this study that the tethered formation will remain in-orbit for an extended period of time.

There have been several proposed ADR methods [2,6–8,11,17] that utilize harpoons, mechanical grapples, or nets to grab the debris object. There has been particularly encouraging results from the Astrium Harpoon system [18] demonstrating the capability to cleanly penetrate metal while supporting large loads. While the study of the debris capture system is beyond the scope of this research, all of these methods are likely to use tethers to connect the debris to the ADR craft because tethers are a very effective means to change the orbital momentum of on-orbit objects.

One of the primary challenges of the tethered-tug system is collision avoidance between the end bodies. During the thrusting maneuver the tether is strained. When the thrust is no longer present the tether will restore itself to zero strain, pulling the tug and debris together. References [11,12] show the strain–collision behavior in more detail. Therefore, it is important to reduce post-thrust strain and relative motion between the bodies to reduce the collision potential. This is done through input shaping of the open-loop thrust profile. An input shaped control or thrust profile can be designed such that the primary natural frequency(ies) of the flexible body are not excited by the control input [19,20]. Fig. 2 shows the thrusting profiles considered in this paper including a step input (Fig. 2(a)) and a continuously notched input (Fig. 2(b)). These two thrusting profiles are discussed in Reference [12], and are the baseline performance to which the new results are compared. The step-input represents a thruster being on for a finite burn and then turned off again. This will excite all flexing modes, and can lead to erratic post-burn dynamics. The continuously notched thrusting profile requires a continuously variable thrust magnitude setting, but provides much smoother post-burn dynamics. A challenge implementing such profiles is that many thruster designs only have on/off capabilities. However, a continuously variable thrust profile could be achieved with a solid motor rocket. The challenge of implementing input shaping with thrusters with discrete on–off capabilities motivates the work in this paper. Fig. 2(c) illustrates a new discrete thrust level profile which could be implemented with a cluster of on–off thrusters. Finally, an impulsive/bang–bang method is considered as shown in Fig. 2(d). Here a single on–off thruster is considered, but time delays are added between the active periods to achieve the desired input shaping.

There have been multiple studies of input shaping on flexible bodies, primarily led by Singhose or Singh [19–25]. Jasper and Schaub [12] demonstrate the effectiveness of an input shaping strategy using a continuously varying thruster profile on the tethered-tug system while creating a very robust control to uncertain debris mass. However, this continuous, smooth thrust profile is unachievable by current-day liquid chemical engines, but could be achieved a solid motor with the desired core design. The post-burn dynamics is improved relative to the step-input with reduced jerk on the tether attachments and faster settling times onto a smooth nadir-aligned oscillation or tumble about nadir. This motivates exploring discretized and bang–bang input shaping thrust profiles. The discretized thruster profile could be implemented with a cluster of thrusters. For example, having 3 thrusters that can be turned on individually would provide 3 discrete levels of thrust. The bang–bang thruster profile with time delays would be suitable for a single on–off thruster implementation. Watanabe et al. [26] and Singhose [19] have also specifically demonstrated input shaping for tethered systems. These studies focus on convolution of multiple impulses to achieve the desired performance. This paper expands upon these studies by analyzing convolution of multiple delay transfer functions, known as a Posicast system, and how such

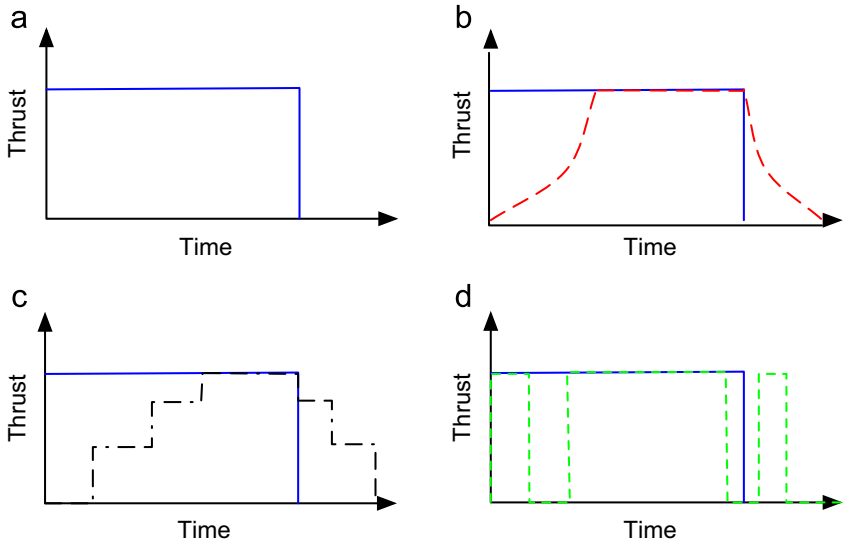

Fig. 2. Example thrust profiles considered. (a) Step-input thrust profile. (b) Continuous notch thrust profile. (c) Discretized notch and Posicast thrust profile. (d) Impulsive thrust profile.

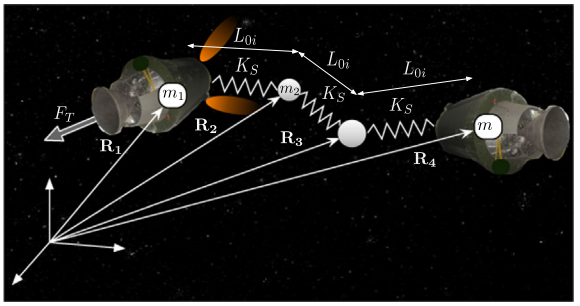

Fig. 3. Discretized tether model example with 2 tether masses.

an open-loop deorbiting thrust profile is applicable for space-based towing applications. Bang–bang input shaping is also explored in high-thrust environments with rigid body end masses. The effectiveness of the discrete input shaping methods are analyzed in deep-space simulations to understand the difference in performance between each method. On-orbit studies are then explored to consider the low Earth orbit ADR application.

2. Tethered-tug system model

The tethered-tug system consists of a thrusting vehicle, the object to tow, and a tether between the two (Fig. 1). The tug and the towed object are modeled as rigid bodies that are capable of rotation and translation. The tether is then discretized into multiple lumped point masses connected by visco-elastic forces, when in tension, as shown in Fig. 3.

The tether starts taut at the beginning of thrusting in this study because a slack tether results in an undesirable whipping behavior [11,12]. Reference [27] shows that small amounts of initial pre-tension have a minimal impact on the resulting post-burn dynamics. Further, the thrusting body has active attitude control to ensure that the thrust vector points are in the desired direction, while thrusting occurs. The attitude control is turned off when the thruster is off.

This research focuses on the gross behavior of a tethered end bodies which can be adequately described with discretely lumped masses which approximate the tether flexing and whipping. Discrete-mass representations of tethers are used frequently [28–32]. The tethered-tug concept considers a formation with large rigid body end masses, where maintaining tension in the tether is not enforced. Slack-taut tether behavior with rigid end bodies is a fairly unexplored area of research especially when large thrust maneuvers are also applied to the system.

The translational equations of motion, caused by the tether, for the system in Fig. 3 can be expressed as

$$\begin{aligned}
\ddot{\boldsymbol{R}}_i &= \frac{1}{m_i}(K_S(|\boldsymbol{R}_{i+1}-\boldsymbol{R}_i|-L_{0,i})\hat{e}_{i,i+1})\\
\ddot{\boldsymbol{R}}_{i+1} &= \frac{1}{m_{i+1}}(K_S(|\boldsymbol{R}_{i+2}-\boldsymbol{R}_{i+1}|-L_{0,i+1})\hat{e}_{i+1,i+2}-m_i\ddot{\boldsymbol{R}}_i)\\
&\vdots\\
\ddot{\boldsymbol{R}}_N &= \frac{1}{m_N}(-K_S(|\boldsymbol{R}_N-\boldsymbol{R}_{N-1}|-L_{0,N})\hat{e}_{N-1,N})
\end{aligned} \tag{1}$$

where N is the number of masses and $\hat{e}$ defined as

$$\hat{e}_{i,j} = \frac{\boldsymbol{R}_j-\boldsymbol{R}_i}{|\boldsymbol{R}_j-\boldsymbol{R}_i|} \tag{2}$$

These are only part of the equations of motion used for the numerical simulation used in this paper. Gravity and the thrust control acceleration are also present as well as the rigid body dynamics for the tug and debris.

The natural frequency ω_n of the system can be found by taking the complicated three-dimensional model in Fig. 3 and simplifying it to a one-dimensional problem, as in Fig. 4. See References [12,27] for the full derivation.

The spring constant K_S is expressed as

$$K_S = \frac{EA}{L_0} \tag{3}$$

with units of N/m. Here L_0 is the initial, unstretched (equidistant) length of the tether between each mass, E

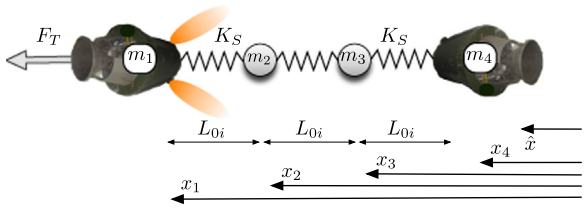

Fig. 4. One-dimensional, linearized tether model.

is Young's modulus of elasticity for the tether, and A is the cross sectional area. Because Eq. (1) models a tether as a spring, it is *only accurate while the tether is in tension. When the separation distance is less than* L_0, *all spring forces go to zero*. The eigen values of the system in Eq. (1) are then found to get the natural frequencies of the system [12], which are used in the input shaping profiles discussed in Section 3.

3. Tug thruster inputer shaping methods

3.1. Continuous input shaping overview

Reference [12] shows that the first fundamental mode of the tethered tug system causes the most motion between the bodies. By creating a doubly notched thrust profile, where the notched frequencies span a range around the fundamental mode, leads to a robust control design that can withstand errors in knowledge of the mass of the towed object (debris mass is not well known in advance). The double notch filter is used throughout this paper for the 'continuous' and 'discrete' notch thruster magnitude shaping cases.

A double notch is effectively created by notching two frequencies at once or by multiplying two notch filters together, in the frequency domain, that have different cut-off frequencies. This places two zeros around the primary pole of the system:

$$g(s)=\frac{(s^2+\omega_{c1}^2)(s^2+\omega_{c2}^2)}{(s^2+\mathrm{BW}_1 s+\omega_{c1}^2)(s^2+\mathrm{BW}_2 s+\omega_{c2}^2)} \tag{4}$$

where s is the frequency, ω_{c1} is the first cut-off or notch frequency, ω_{c2} is the second cut-off or notch frequency, and $BW1$ and $BW2$ are the bandwidths for each notch, respectively. For a more in-depth explanation on the operation of the double notch, see Reference [12].

While some solid rocket cores could be designed to give a continuously varying thrust profile, liquid engines have limited capability to have continuously varying thrust. Generally, the range of the throttle is not large enough for an ADR mission and would require significant new development of liquid engine capability to achieve a notched thrust profile. Because of this fact, three other thrusting methods with discrete thrusting levels are considered next.

3.2. Discretized thrust input shaping

First, a simple method called the discretized input shaping control is considered where the continuous input shaping solution is discretized to a set of discrete thrust levels. For example, with a cluster of 4 identical thrusters, the open-loop towing control is only capable of stepping the net thrust in 25% increments of the maximum thrust available. This is implemented by having each thruster individually turn on or off at the desired times. The continuous model is used as the desired thrust profile but the actual profile is set to specific magnitudes given a thrust step size. The basic algorithm is given as follows:

$$\text{step size} = T_{\text{step}} \tag{5a}$$

$$\text{desired thrust} = T_{\text{desired}} \tag{5b}$$

$$\tau_{\text{ratio}} = \text{Mid}-\text{Point Rounding}\left(\frac{T_{\text{desired}}}{T_{\text{step}}}\right) \tag{5c}$$

$$T_{\text{applied}} = \tau_{\text{ratio}} * T_{\text{step}} \tag{5d}$$

The algorithm uses a simple rounding method. The rounding scheme in Eq. (5) uses a mid-point method so that if the desired thrust is greater than 50% of T_{step}, then the applied thrust will jump to the next step size, otherwise the applied thrust remains at the previous level. This causes the desired thrust to be *above* each step size to achieve a new T_{applied} level. The difference between the continuous and discrete applied thrust is demonstrated in Fig. 6.

3.3. Posicast input shaping

As shown by Singh [20], a time delay system can be used as an open loop control on a system:

$$A_0+\sum_{i=1}^{N} A_i e^{-sT_i}=0 \tag{6}$$

Singh demonstrates a number of Posicast methods to properly actuate a system, as well as make the control more robust to modeling errors. Singh also generally considers moving a system from one position to another. However, this paper expands upon these works by formulating a robust Posicast, open-loop input shaper, that achieves a desired velocity without exciting natural frequencies. Because the first mode of the tethered system has been shown to be the most important [12], a Posicast controller is developed only for the first mode.

The Posicast input shaping profile operates on the assumption that a step input control/thrust profile is given to the controller. The controller then takes the step and manipulates it so that it does not excite undesirable modes. The thrust profile created by the Posicast control is shown in Fig. 6 but in the time scale shown, it is harder to differentiate between the impulsive profiles and the step input. It should be emphasized that the Posicast profile *does* behave similarly to the illustration in Fig. 2(c).

Assuming that there are only two end bodies with a spring force between them, the equations of motion are simplified to (*only while in tension*):

$$\ddot{x}_1=\frac{1}{m_1}(K(x_2-x_1-L_0)-F_T) \tag{7a}$$

$$\ddot{x}_2=\frac{1}{m_2}(-K(x_2-x_1-L_0)) \tag{7b}$$

The separation distance between the two end bodies is defined as $L=x_2-x_1-L_0$, where L_0 is the unstretched length, a constant. The resulting tether flexing dynamics is written as

$$\ddot{L}=\ddot{x}_2-\ddot{x}_1 \tag{8a}$$

$$\ddot{L}=-K\frac{m_1+m_2}{m_1m_2}L+\frac{F_T}{m_1} \tag{8b}$$

where $\sqrt{K((m_1+m_2)/m_1m_2)}$ is the natural frequency of a two body spring–mass system. Taking the Laplace transform of the system in Eq. (8) gives the following transfer function:

$$H(s)=\frac{L}{u(s)}=\frac{1}{s^2+K\frac{m_1+m_2}{m_1m_2}} \tag{9}$$

Eq. (9) shows that the poles of the system occur at

$$s=\pm\sqrt{-K\frac{m_1+m_2}{m_1m_2}}=\pm j\omega_n \tag{10}$$

where $j=\sqrt{-1}$. The most basic Posicast controller uses only one time delay and is solved as an example. A single delay takes the form:

$$A_0+A_1e^{-sT}=0 \tag{11}$$

Substituting s in Eq. (10) into Eq. (6) and using Euler's equation, the exponential term can be written as

$$e^{j\omega_nT}=\cos(\omega_nT)+j\sin(\omega_nT) \tag{12}$$

To solve the system, Eq. (12) is separated into real and imaginary components:

$$\text{Real:}\quad A_0+A_1\cos(\omega_nT)=0 \tag{13a}$$

$$\text{Imaginary:}\quad A_1\sin(\omega_nT)=0 \tag{13b}$$

This quickly results in the solutions for A_0 and T if A_1 is defined to equal 1, the maximum normalized input:

$$T=(2n-1)\frac{\pi}{\omega_n} \tag{14a}$$

$$A_0=-\cos(\omega_nT)=-\cos((2n-1)\pi) \tag{14b}$$

However, the time delay control in Eq. (11) is very sensitive to modeling errors therefore several delays are given to make the system more robust. To make the system solvable, Singh [20] specifies that each time delay is only a multiple of the single delay T, from Eq. (14). The controller designed for the tethered tug system is

$$A_0+A_1e^{-sT}+A_2e^{-2sT}+A_3e^{-3sT}+A_4e^{-4sT}=0 \tag{15}$$

To solve this system for the impulse amplitudes, A_i, several equations are required. Note that implementing the system in Eq. (15) would require 5 thrusters, one for each amplitude A_i. The real and imaginary parts are found again, as in Eq. (13). However three more constraints are defined:

$$\frac{\mathrm{d}}{\mathrm{d}\omega_n}(\text{Real})=0 \tag{16a}$$

$$\frac{\mathrm{d}}{\mathrm{d}\omega_n}(\text{Imaginary})=0 \tag{16b}$$

$$A_0+A_1+A_2+A_3+A_4=1 \tag{16c}$$

The derivatives of the real and imaginary components of Eq. (15) add robustness by reducing the size of the residual vibration, with respect to variations in the tethered system natural frequency ω_n after an input has been added. The constraint that all of the amplitudes sum to one is used so that the input is not scaled but equal to its full value after all delays have occurred. Solving this system of equations, the amplitudes are found to be

$$A_0=\frac{1}{16}\csc\left(\frac{T\omega_n}{2}\right)^4 \tag{17a}$$

$$A_1=-\frac{1}{4}\cos(T\omega_n)\csc\left(\frac{T\omega_n}{2}\right)^4 \tag{17b}$$

$$A_2=\frac{1}{8}(2+\cos(2T\omega_n))\csc\left(\frac{T\omega_n}{2}\right)^4 \tag{17c}$$

$$A_3=-\frac{1}{4}\cos(T\omega_n)\csc\left(\frac{T\omega_n}{2}\right)^4 \tag{17d}$$

$$A_4=\frac{1}{16}\csc\left(\frac{T\omega_n}{2}\right)^4 \tag{17e}$$

To turn this development into a velocity control instead of a position control, the amplitudes from Eq. (17) are used at the beginning and end of the step input thrust profile to achieve a ramping on and off as shown in Fig. 2(c). The amplitudes increase, summing from A_0 to A_4, hold at the maximum amplitude of the input for the thrust duration, and then decrease from A_4 to zero. For example, a three thrust velocity control would require

$$\begin{aligned}
&t=0 \quad \text{Thrust}=A_0\\
&t=T \quad \text{Thrust}=A_0+A_1\\
&t=2T \quad \text{Thrust}=A_0+A_1+A_2\\
&t=T_{\text{burn}} \quad \text{Thrust}=A_0+A_1\\
&t=T+T_{\text{burn}} \quad \text{Thrust}=A_0\\
&t=2T+T_{\text{burn}} \quad \text{Thrust}=0
\end{aligned} \tag{18}$$

Here, T_{burn} is the approximate burn time required to achieve the desired Δv. The duration of the burn is nearly the same as the step input but is extended by 8 T to account for the ramp on/off behavior of the 5 time delay system.

To demonstrate why a 5 thrust level system is used in Eq. (15), versus the two impulse version of Eq. (11), their expected vibration amplitudes are compared. These amplitudes can be expressed as [19]

$$A=\sqrt{\sum_{i=0}^{B}(A_i\cos(\omega_nT_i))^2+\sum_{i=0}^{B}(A_i\sin(\omega_nT_i))^2} \tag{19}$$

where T_i are the times of the impulses A_i and ω_n is the natural frequency. (For the 2 impulse case, i goes to $B=2$ while i goes to $B=5$ for the 5 impulse case.) Summing these up over a range of natural frequencies, due to uncertain debris mass, the expected response of each system can be demonstrated. Fig. 5 shows the percentage of remaining vibration in the tethered-tug system, given the two different Posicast controls. It is clear from Fig. 5 that as debris mass changes, the residual vibration is much smaller for the multi-impulse control, versus the two impulse control. Variations on the order of 40% can be expected from the non-robust

method while the robust 5 impulse control only experiences about 0.3% variation across the expected mass range. Thus, the 5 impulse control is a major improvement.

Fig. 5 also shows the effect of the constraints in Eq. (16). The robust Posicast, Fig. 5(b), has a much more flat response to changes in debris than the 2 thrust level control, Fig. 5(a). By setting the real and imaginary components of the transfer function to zero, the control removes the system response at the expected system modes. Zeroing the derivatives of the transfer function flattens the response of the Posicast to a wider range of system properties.

3.4. Bang-off-bang input shaping

The bang-off-bang controller creates a profile that can be implemented by a single thruster that can repeatably be turned on and off. This method also assumes that a step input is given to the controller that is then modified to not excite system modes. Singh [20] demonstrates several ways to create a bang-off-bang controller; however, the basic principle is to find a linear system's state transition matrix and control matrix. Combining these matrices with several constraints, like those in Eq. (16), yields a system that can be solved as a linear programming problem. Full details are given by Singh, however, an abbreviated derivation is given for clarity. Further, the thrust profile is shown in Fig. 6 but is better illustrated in Fig. 2(d).

Given initial and final conditions, $\boldsymbol{x}_0$ and $\boldsymbol{x}_f$ and the linearized system derived from Eq. (1), the problem can be set up as follows. We wish to minimize the maneuver time, so

$$\text{Minimize } f^T t \tag{20}$$

where t is the maneuver time vector and f is a vector that defines the given time we wish to minimize. In this case, since it is desired to minimize the total time, f is a vector of zeros except the last value, which is a one corresponding to the last time. Singh then discretizes the continuous equations of motion, linearized from Eq. (1), obtaining:

$$\boldsymbol{x}_{k+1} = [A_D]\boldsymbol{x}_k + [B_D]\boldsymbol{u}_k \tag{21}$$

where $[A_D]$ is the discrete dynamics matrix and $[B_D]$ is the discrete control matrix. Writing the system in terms of the initial condition:

$$\boldsymbol{x}_{k+1} = [A_D]^k \boldsymbol{x}_0 + \sum_{i=1}^{k} [A_D]^{k-i}[B_D]\boldsymbol{u}_i \tag{22}$$

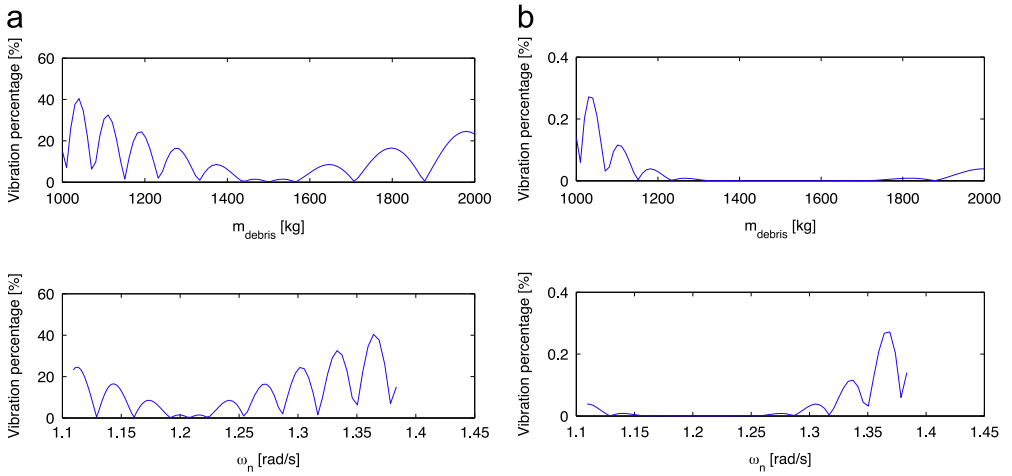

Fig. 5. Residual vibration (percentage) from each Posicast method through evaluation of Eq. (19). Debris mass varies between 1000 kg and 2000 kg (nominal at 1500 kg, $\omega_n = 1.21$ rad/s). Deep space. (a) Two thrust level Posicast, Eq. (11). (b) Five thrust level (robust) Posicast, Eq (15).

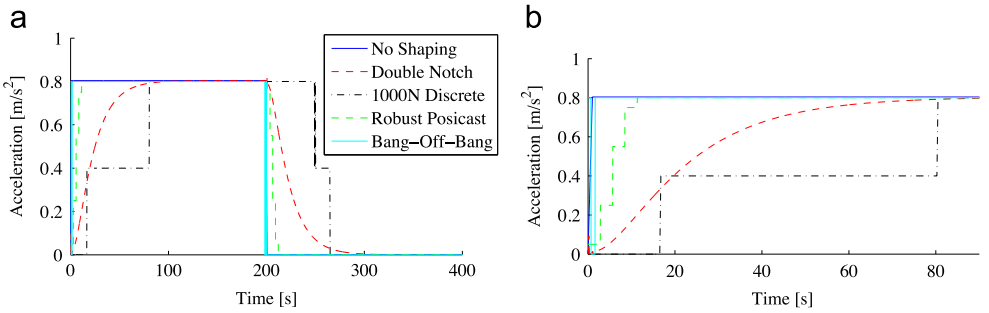

Fig. 6. Applied thrust profiles with different input shaping techniques. (a) Full thrust profiles. (b) Thrust profiles as they turn on.

The summation of inputs can be rewritten and solved for as a matrix giving:

$$\left[[A_D]^{N-1}[B_D]\ \ [A_D]^{N-2}[B_D]\ \ \cdots\ \ [A_D][B_D]\ \ [B_D]\right]\begin{bmatrix} u_1 \\ u_2 \\ \vdots \\ u_N \end{bmatrix} = \boldsymbol{x}_f - [A_D]^N \boldsymbol{x}_0 \tag{23}$$

or equivalently

$$[M(A_D, B_D)]\boldsymbol{u} = b(\boldsymbol{x}_0, \boldsymbol{x}_f, [A_D]) \tag{24}$$

The system given in Eq. (23) allows the user to specify the initial and final conditions ($\boldsymbol{x}_0$, $\boldsymbol{x}_f$) and it is solvable using linear programming techniques, in the form of $M\boldsymbol{u} = b$. However, to be useful as a bang-off-bang system, several additional constraints are required. One is that the inputs end in either zero or one. This is enforced by adding a row to [M] that is all zeros except for the last column, which is a one. The [b] matrix also has an additional value added to the end that is either a zero or one. This allows for the final control value u_N to be specified as whatever value is designated in [b], off (0) or on (1). The second constraint is on the input sizes. To create a bang-off-bang control, the inputs $\boldsymbol{u}$ are required to be bounded between zero and one. The value of one is used so that the user defined input is used in its entirety and not scaled. For this particular implementation, the system is discretized into more than 300 steps over the minimum cost time determined by the linear programming routine. The large number of discretizations (over only several seconds for each ON or OFF segment) allows accuracy in the solution. If the discretization size were bigger, poor results can ensure.

To create a velocity control bang-off-bang profile, the linear programming problem is solved twice. To begin thrusting while avoiding exciting system modes, $\boldsymbol{x}_0 = 0$, $\boldsymbol{x}_f = L_1$, and the final input u_N is specified to be 1.

The value L_1 is defined simply from the approximate separation distances seen from the other control methods, like the continuous notch. The tether usually ends up stretching less than a meter, for a 1000 m tether. The selection of this value does not drastically affect the performance of the system, unless it is larger than the stretch distance possible given the thrust magnitude and the tether material properties. The final control input is kept at one for the burn duration to achieve the desired Δv. The linear programming problem is then solved again to end thrusting using $\boldsymbol{x}_0 = L_1$, $\boldsymbol{x}_f = 0$, and the final input u_N is specified to be 0. The beginning and ending bang-off-bang profiles are then placed at the beginning and end of the step input thrust profile. This allows for proper relative motion reduction with the desired Δv. The exact thrust profile used is shown in Fig. 6 however the switch times are small enough that they are hard to see on the time scale shown.

4. Numerical simulation results

To demonstrate the effectiveness of each thrusting method (continuous, discretized, and impulsive), numerical simulations are performed. The basic system parameters (mass, size, inertia, thrust abilities) are given in Table 1 and are modeled after a Soyuz upper stage for the tug vehicle, and a Cosmos rocket body for the debris object. These numerical simulation conditions are motivated by the original development of this concept to remove Cosmos upper stages. The input shaping methodology presented in this paper is general and applies to much larger debris objects being towed as well. With larger masses, the eigenfrequencies will change, and the thrusting profiles must be modified accordingly.

Table 1
Vehicle, tether and simulation parameters.

Tug mass	2500 kg
Tug inertia	diag[10,208, 10,208, 2813] kg m^2
Debris mass	1500 kg
Debris inertia	diag[1285, 6829, 6812] kg m^2
Tether length	1000 m, equal space between masses
Tether material	Kevlar
E	1470 GPa
Tether diameter	3.2 mm
Tether mass	11.822 kg[a]
Thrust	2009 N
Δv	100 m/s
Starting altitude	800 km (circular)

[a] http://www.matweb.com/index.aspx.

Given the values in Table 1, the natural frequencies of the system are obtained. It is interesting to note that the fundamental frequency is the same between the two-body, three-body, or four-body cases. This turns out to be (for two bodies: $m_1 = 2500$ kg, $m_2 = 1500$ kg; for three bodies: $m_1 = 2500$ kg, $m_2 = 11.82$ kg, and $m_3 = 1500$ kg, for four bodies: $m_1 = 2500$ kg, $m_{2a} + m_{2b} = 5.91 + 5.91 = 11.82$ kg, and $m_3 = 1500$ kg) at $\omega_{n1} = 0.19$ Hz. The three node case also has its second mode at $\omega_{n2} = 3.43$ Hz. The first mode is of greatest concern and is the frequency that all input-shaping methods attempt to reduce. With the values in Table 1 the resulting input-shaped thrust profiles are shown in Fig. 6.

For the simulations, several implementation features should be noted. First, the trapezoidal difference method [33] is used to transform from frequency to discrete time domains. The attitude on the tug (m_1) is maintained while thrusting occurs. The discretized notch filter uses a midpoint round up discretization (Eq. (5)). Finally, the Δv applied is equal to 100 m/s (about 120 kg of fuel). Based upon input-shaping method, this can vary the thrusting duration. The time T that results from Eq. (14), and is used to implement the profiles of Eqs. (15) and (23), is about 2.83 s. This means that the Posicast amplitudes change, and the bang–bang profile switches use T as the baseline actuation time. For a five step Posicast system, the ramp on or off takes just over 14 s.

4.1. Deep space results

Deep space simulations (in the absence of a gravity field) are conducted because they are informative for showing the effectiveness of a given thrusting method. Deep space is also relevant for the asteroid towing concept

(Fig. 1(b)). When a step input thrust profile is used, as in Fig. 2(a), it excites all modes present in the flexible tether system causing relative motion between the two bodies. In deep space, this generally results in a collision. However, input shaping the thrust profile can remove these excitable frequencies from the thrust profile, reducing the relative motion. This is demonstrated in Fig. 7. Note that the tether tension profile behaves similarly to the thrust profile. Further, there is almost no relative motion between the two end bodies, as shown by the separation distance remaining near 1000 m. Fig. 7 also considers the double notch with a mass knowledge error of 500 kg (the debris is expected to be 2000 kg but it is really 1500 kg), again showing the effectiveness of this method.

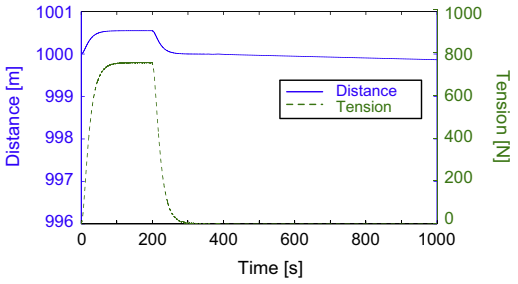

Fig. 7. Deep space relative motion and tether tension response between tug and debris using a *continuous* double notch spanning $0.14 \le \omega_c \le 0.22$ Hz. Expected debris mass of 2000 kg ($\omega_n = 0.17$ Hz), actual mass is 1500 kg ($\omega_n = 0.19$ Hz). 2009 N thrust, with 2 discrete tether masses.

Fig. 8 shows four non-continuous thrust system responses. (Fig. 6 gives the profiles used.) In Fig. 8(a) and (b) the continuous notch profile used to generate Fig. 7 has been discretized into 100 N and 1000 N steps, respectively. The 100 N step size was chosen to study a relatively small discretization that could follow the desired continuous profile somewhat effectively. The 1000 N step size was chosen because it is much more likely that a realistic thruster is capable of a small range of different thrusts. A ~2000 N thrust could be attained by coupling two, 1000 N thrusters and turning them on at desirable times.

Altering the continuous thrust profile to discrete steps, Fig. 8(a) and (b), is moderately effective in reducing post-burn relative velocity even when introducing these discrete thrusting steps. The 100 N discretization sees greater than 900 m of separation between the two end bodies, showing that there was only a small amount of tension remaining in the tether at the end of the thrusting duration. However, the much cruder 1000 N discretization of the continuous thrust profile experiences much more relative motion, and the system collapses to 570 m after 1500 s. This shows the 1000 N discretization appears to be too crude of a discretization, even though it is more practical for current-day engine capabilities.

When considering the impulsive input shaping methods in Fig. 8(c) and (d), it can be seen that these thrust profiles (Fig. 6) produce more desirable behavior. The Posicast controller only sees about 7 m of drift over the time span considered, while the bang-off-bang profile sees about 100 m of drift. These results are exciting because

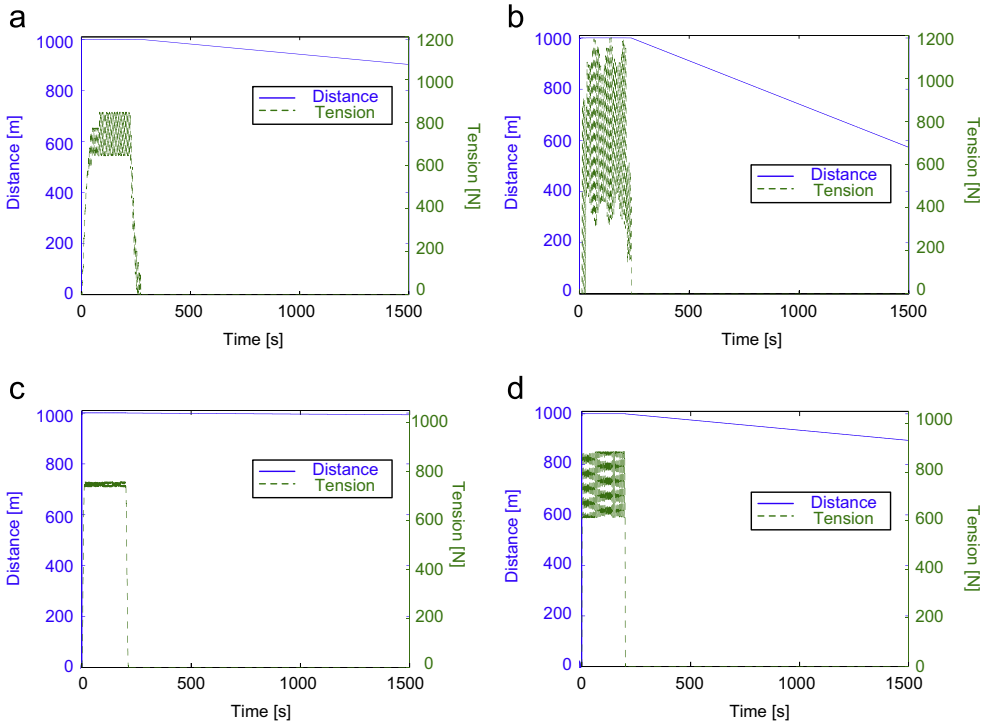

Fig. 8. Relative motion and tether tension response between tug and debris. Expected debris mass of 2000 kg ($\omega_n = 0.17$ Hz), actual mass is 1500 kg ($\omega_n = 0.19$ Hz, green line(s) oscillation frequency). 2009 N thrust, with 2 discrete tether masses. (a) 100 N step *discrete* double notch spanning $0.14 \le \omega_c \le 0.22$ Hz. (b) 1000 N step *discrete* double notch spanning $0.14 \le \omega_c \le 0.22$ Hz. (c) Robust Posicast thrust shaping, Eq. (15). (d) Bang-off-bang thrust shaping, Eq. (23). (For interpretation of the references to color in this figure caption, the reader is referred to the web version of this paper.)

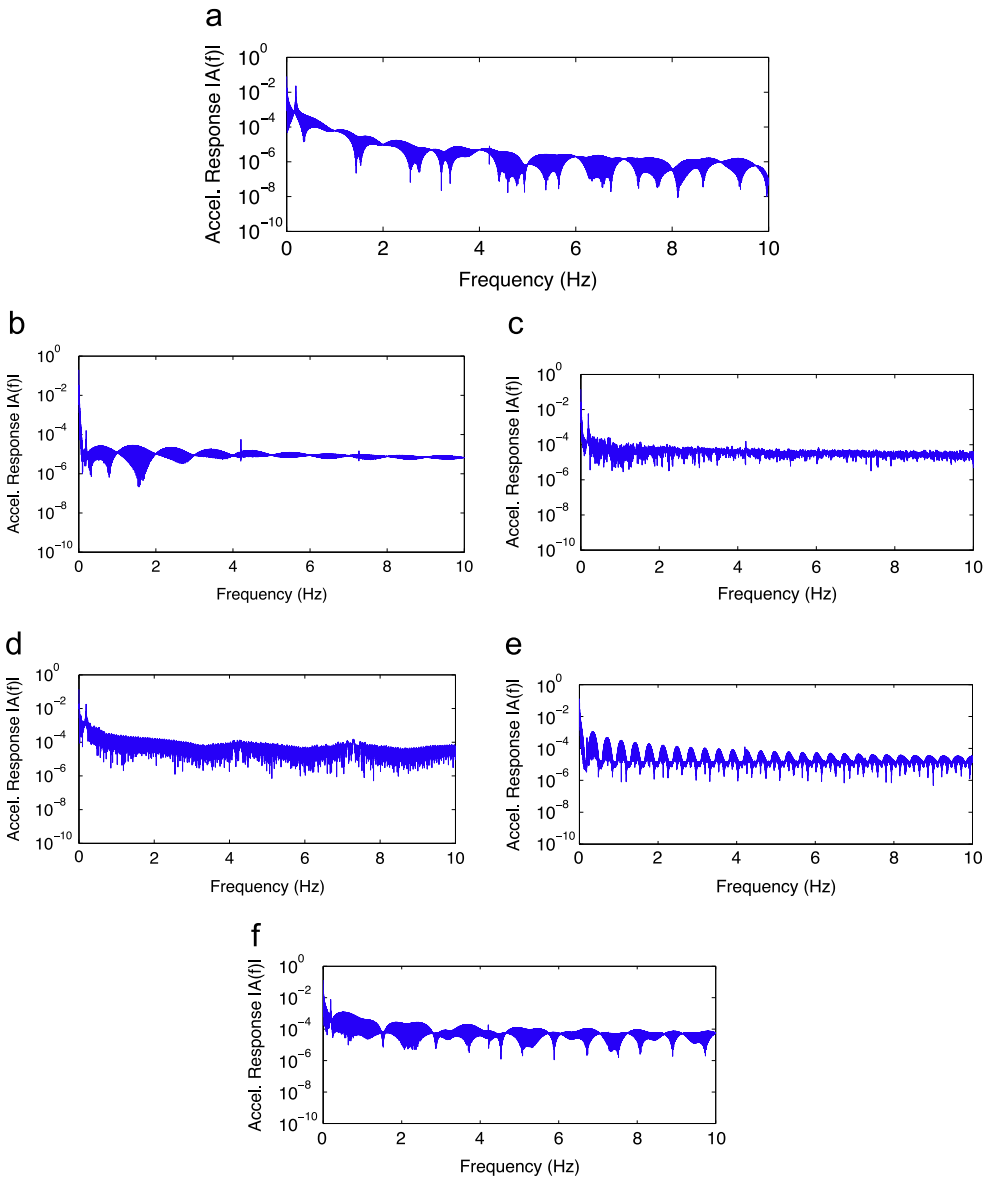

Fig. 9. Tug vehicle frequency response to 2009 N thrust, with 2 discrete tether masses, in deep space. (a) Step-input thrust profile. (b) Double notch spanning $0.14 \leq \omega_c \leq 0.22$ Hz. (c) 100 N discretized double notch spanning $0.14 \leq \omega_c \leq 0.22$ Hz. (d) 1000 N discretized double notch spanning $0.14 \leq \omega_c \leq 0.22$ Hz. (e) Robust Posicast thrust shaping. (f) Bang-off-bang thrust shaping.

they demonstrate that input shaping controllers can be designed with profiles that are more reasonable for current-day engine capabilities.

Fig. 9 shows the frequency domain response of the tug mass, given the different thrust profiles. Fig. 9(a) shows a step input exciting the modes of the tethered-tug system. The primary mode occurs at 0.19 Hz and has a fairly large magnitude. The double notch in Fig. 9(b) reduces this first mode by about two orders of magnitude in power, thus creating the tiny relative motion in Fig. 7. The magnitude of the first mode in the 100 N discretized frequency response Fig. 9(c) is only slightly attenuated from the step input. However, this is enough to produce small relative motion, as shown by Fig. 8(a). The 1000 N discretization response Fig. 9(d) has very little difference from the step input, and therefore experiences a post-burn collision quite quickly. Fig. 9(e) shows the Posicast frequency response, which also shows a very attenuated fundamental mode (0.19 Hz), comparable to the continuous double notch in Fig. 9(b). This again demonstrates that impulsive input shaping is a viable method to controlling the tethered-tug system. While some other frequencies do appear amplified, they are not around the fundamental mode of the system, and therefore do not adversely affect the system as modeled. Fig. 9(f) shows the bang-off-bang frequency response which does not see nearly as much attenuation as the Posicast or double notch profile, but it does attenuate the fundamental mode enough to see

reduced relative motion between the two bodies, as shown in Fig. 8(d).

4.2. On-orbit results

Deep space simulations motivate the use of a given thrust profile for on-orbit analyses. However, the orbital dynamics create interesting behavior that is not predicted by deep space analysis, including the tendency toward a tumbling formation or a gravity gradient – nadir – alignment, of the tethered system [12]. Even though the 100 N discretized thrust profile had better performance in a deep space environment, it is not a realistic performance for a thruster. Therefore, the 1000 N discretization is used in the on-orbit analysis. The 1000 N discretized, robust Posicast, and bang-off-bang thrust profiles are used, unaltered from their deep-space implementation.

Fig. 10 shows the relative separation distance and tension present in the tethered-tug system for a continuous and discrete notch, as well as the two impulsive shaped thrust profile.

While a step input thrust profile will transit between periods of tension and slack, with highly dynamic behavior, the double notch Fig. 10(a) experiences a slow and steady drift. The periodic behavior in the drift is from the small eccentricity in the orbit, after the maneuver. This drift is somewhat expected from the deep space results because the relative velocity between the end bodies is quite small and the formation only slowly collapses. The angle from nadir is used as a metric for how well each thrusting method achieves a tumbling motion or nadir alignment. For the drifting notch motion, the end bodies start thrusting aligned with the in-track orbital direction (0°) and the formation essentially stays in that orientation.

This is fairly desirable behavior because the bodies are simply drifting, zeroing tension in the tether and reducing jerk and other strains on the system. The end bodies do pass within a few meters of each other after 9 orbits, but the relative velocities are quite small, reducing risk of debris creation if the bodies did end up bumping. If the applied Δv is large enough, the system could de-orbit while the bodies are still drifting, thus avoiding collisions. The notch thrust profile can also be modified to induce formation rotation through a small additional radial thrust, inducing gravity gradient motion [27].

When considering the non-continuous profiles the behavior can change significantly. The 1000 N discretized thrust profile in Fig. 10(b), that did not work well in deep space, performs moderately in orbit, maintaining more separation distance between end bodies. This is likely due to larger differences in relative motion post-maneuver that cause the two craft to stay further separated. The 1000 N discretized notch also does oscillate about nadir. But, again, the end bodies move significantly with respect to each other, making this motion not explicitly gravity gradient.

Conversely, the robust Posicast in Fig. 10(c) demonstrates admirable performance because the end bodies do not approach each other, as occurs with the continuous double notch in Fig. 10(a), and it is less dynamic than the discretized profile. The Posicast response appears are more benign experiencing lower tension (100 N versus 700 N and 1400 N for the continuous and discrete notch profiles, respectively) and the system quickly settles into a tumble about nadir, with end body separations near the full length of the tether.

Finally, Fig. 10(d) shows the bang-off-bang performance. The bang–bang profile sees significant motion between the

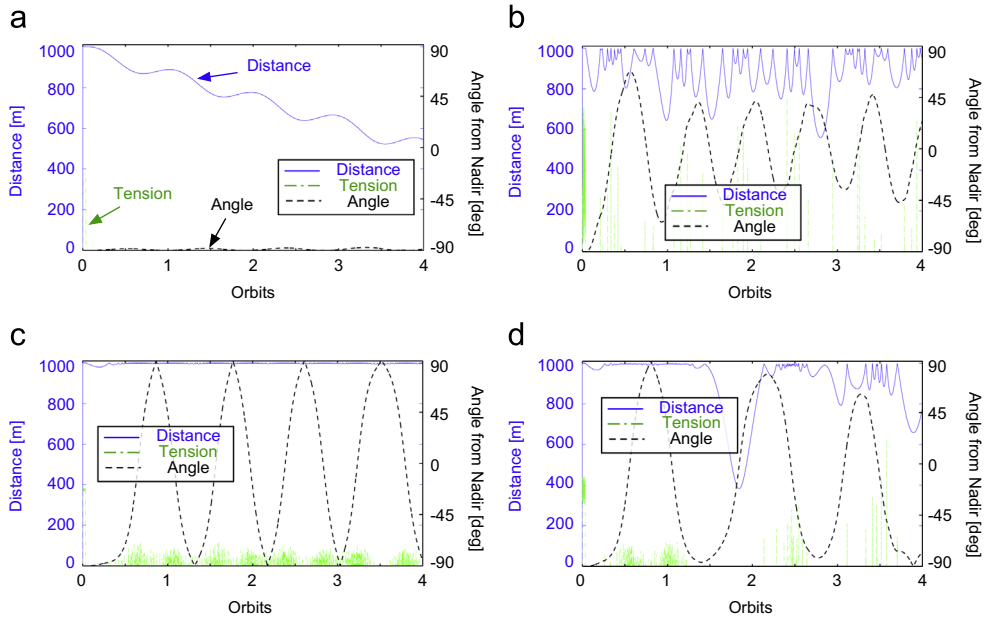

Fig. 10. Relative motion, angle from nadir, and tether tension response between tug and debris for four orbits. Tension scaled by 0.5. Tether $\omega_n = 0.19$ Hz. 2009 N thrust, with 2 discrete tether masses. On-orbit. (a) *Continuous* double notch spanning $0.14 \leq \omega_c \leq 0.22$ Hz., (b) 1000 N *discretized* double notch spanning $0.14 \leq \omega_c \leq 0.22$ Hz. (c) Robust Posicast thrust shaping. (d) Bang-off-bang thrust shaping.

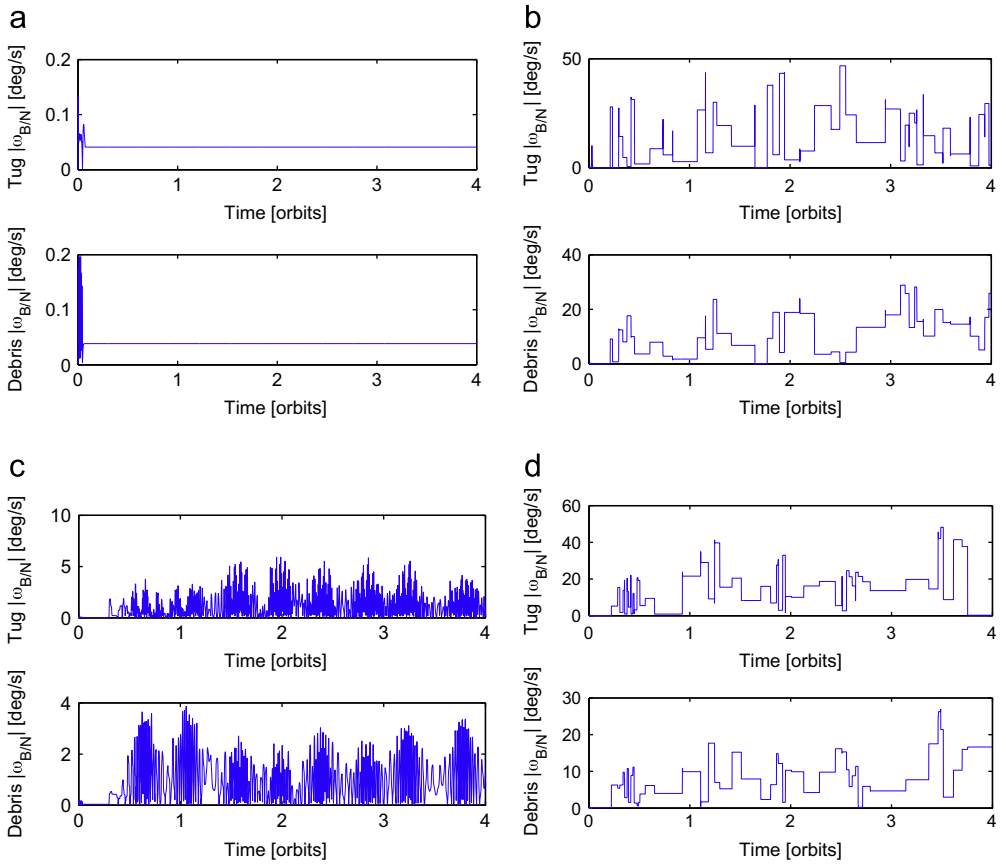

Fig. 11. Notch end body rotation rates over 4 orbits. (a) Double notch spanning $0.14 \le \omega_c \le 0.22$ Hz. (b) 1000 N *discretized* double notch spanning $0.14 \le \omega_c \le 0.22$ Hz. (c) Robust Posicast. (d) Bang-off-bang.

end bodies, however separation distances remain large. Tensions are larger than the Posicast but not extreme. With this profile, the formation does not achieve a consistent angular motion making this neither gravity gradient nor tumbling. The bang-off-bang is not perfect but is much better than a pure step input or the discretized notch.

End body rotation rates are also important when considering performance of an input shaping thrust profile. Rates should ideally be small, avoiding wrap-up in the tether to avoid chaotic spinning or potential wrapping and breaking of protruding objects such as an antenna or solar panels. The rotation rate results are presented in brief to show how each input shaping profile can dramatically affect these rates. Future work will require more study of these behaviors but some performance information can still be gleaned from this study.

A step input will cause large rotation rates in the end bodies due to post-thrust tension often remaining in the tether and large end body relative motion.

Conversely, the notch's performance in Fig. 11(a) demonstrates very small rotation rates, because of the small relative end body motion (drifting). The discretized notch unfortunately does not have similarly small rotation rates, shown in Fig. 11(b). This is not unexpected as the discretized notch profile is literally just a set of step inputs that end up exciting motion in the system. With this relatively poor thrust profile design, these large rates will be the norm, not the exception.

For the Posicast control, Fig. 11(c), the rates are generally less than 5°/s, much smaller than the discretized notch that has rates reaching 45°/s. While the rates in Fig. 11(c) change quickly, it is because the tether is constantly pulling the masses back in alignment. The masses were not observed to complete a full rotation, avoiding the potential of wrapping in the tether. The bang-off-bang profile's end body rotation rates in Fig. 11(d) are fairly large demonstrating challenging dynamics to be studied in the future work.

5. Conclusion

A step input (impulsive) thrust profile is inadequate for a tethered ADR system due to the chaotic motion, collision potential, and relatively high tether tensions induced. The excitement of, primarily, the tether's first mode causes the majority of the relative motion between the end bodies. Open-loop input shaping of only the first mode can largely negate relative motion between the end bodies once the thrust maneuver is performed. This helps the system stay separated in deep space, or achieve a tumbling or gravity gradient motion in orbit. While the continuous notch input shaping performs well by limiting relative velocity between end bodies, it still experiences a collapse in the formation over time. The impulsive Posicast and bang-off-bang profiles are more achievable for high-thrust rockets.

The bang-off-bang profile performs reasonably well in deep space but is not nearly as robust while in orbit. However, the Posicast filter creates desirable tumbling motion, large end body separations, and relatively low end body spin rates. This makes the Posicast control the most attractive input shaping method. Still, this paper shows that a multitude of thrust profiles can be successfully implemented to control this system while avoiding collisions.

Acknowledgments

The authors would like to acknowledge Valery Trushkyakov, Professor in the Department of Aviation and Rocket Building, Omsk State Technical University for his contributions to the tethered rocket body ADR method. The authors would also like to thank Anthony Lima an undergraduate researcher who has helped the authors to visualize better the system and verify the numerical simulation.

References

[1] K. I. for Space Studies, Asteroid Retrieval Feasibility Study, Smithsonian Astrophysical Observatory, Pasadena, California, 2012.
[2] C. Bonnal, C.R. Koppel, Getting rid of large debris: a safe low cost alternative, in: 2nd European Workshop on Active Debris Removal, CNES-HQ, Paper No. 3.2, Paris, France, 2012.
[3] J.-C. Liou, N.L. Johnson, Risks in space for orbiting debris, Science 311 (2006) 340–341.
[4] J.-C. Liou, N. Johnson, N. Hill, Controlling the growth of future leo debris populations with active debris removal, Acta Astronaut. 66 (2010) 648–653.
[5] J.-C. Liou, An active debris removal parametric study for leo environment remediation, Adv. Space Res. 47 (2011) 1865–1876.
[6] D. Alary, Astrium's views on oos & adr, in: European On-Orbit Satellite Servicing and Active Debris Removal Conference, Brussels, Belgium, 2012.
[7] J. Reed, J. Busquets, C. White, Grappling system for capturing heavy space debris, in: 2nd European Workshop on Active Debris Removal, CNES-HQ, Paper No. 4.2, Paris, France, 2012.
[8] I. Retat, B. Bischof, J. Starke, W. Froth, K. Bennell, Net capture system, in: 2nd European Workshop on Active Debris Removal, CNES-HQ, Paper No. 4.3, Paris, France, 2012.
[9] R. Benvenuto, M. Lavagna, Dynamics analysis and gnc design support tool of flexible systems for space debris active removal, in: IAA Conference on Dynamics and Control of Space Systems, IAA-AAS-DyCoSS2-14-09-02, Rome, Italy, 2014.
[10] V.S. Aslanov, V.V. Yudintsev, Dynamics of large debris removal using tethered space tug, Acta Astronaut. 91 (2013) 149–156.
[11] L. Jasper, H. Schaub, C. Seubert, T. Valery, E. Yutkin, Tethered tug for large low earth orbit debris removal, in: AAS/AIAA Astrodynamics Specialists Conference, Paper No. AAS 12-252, Charleston, SC, 2012.
[12] L. Jasper, H. Schaub, Input shaped large thrust maneuver with a tethered debris object, Acta Astronaut. 96 (March–April) (2014) 128–137.
[13] V.S. Aslanov, V.V. Yudintsev, Dynamics of large debris connected to space tug by a tether, J. Guid. Control Dyn. 36 (2013) 1654–1660.
[14] ELV-System-Team, Active debris removal by vega upper stage adaptation, in: e.Deorbit Symposium, AO-13780, Langelaan, The Netherlands, 2014.
[15] D. Zimpfer, P. Kachmar, S. Tuohy, Autonomous rendezvous, capture and in-space assembly: past, present and future, in: 1st Space Exploration Conference: Continuing the Voyage of Discovery, AIAA 2005-2523, Orlando, FL, 2005.
[16] Y. Makarov, A. Ronse, V. Trushlyakov, The use of adapted upper stages for the removal of satellite and rocket body debris from unstable orbital regions, in: 62nd International Astronautical Congress, IAC-11,A6,5,10,x10020, Cape Town, South Africa, 2011.
[17] V. Trushlyakov, J. Makarov, G. Raykunov, J. Shatrov, D. Baranovo, The development of autonomous onboard systems for the controlled deorbiting of stages separating parts of space launch vehicle, in: 2nd European Workshop on Active Debris Removal, CNES-HQ, Paper No. 2.5, Paris, France, 2012.
[18] J. Reed, S. Barraclough, Development of harpoon system for capturing space debris, in: Sixth European Conference on Space Debris, Darmstadt, Germany, 2013.
[19] W. Singhose, Command shaping for flexible systems: a review of the first 50 years, Int. J. Precis. Eng. Manuf. 10 (2009) 153–168.
[20] T. Singh, Optimal Reference Shaping for Dynamical Systems, Theory and Applications, CRC Press, Boca Raton, Florida, 2010.
[21] T. Singh, P. Singla, U. Konda, Polynomial chaos based design of robust input shapers, J. Dyn. Syst. Meas. Control 132 (2010). 051010-1–13.
[22] R. Kumar, T. Singh, Design of input shapers using modal cost for multi-mode systems, Automatica 46 (2010) 598–604.
[23] W. Singhose, W. Seering, N. Singer, Residual vibration reduction using vector diagrams to generate shaped inputs, J. Mech. Des. 116 (1994) 654–659.
[24] W. Singhose, S. Drezinski, N. Singer, Extra-insensitive input shapers for controlling flexible spacecraft, J. Guid. Control Dyn. 19 (1996) 385–391.
[25] W.E. Singhose, A.K. Banerjee, W.P. Seering, Slewing flexible spacecraft with deflection-limiting input shaping, J. Guid. Control Dyn. 20 (1997) 291–298.
[26] T. Watanabe, T. Makida, H.A. Fujii, H. Kojima, W. Singhose, An application of input shaping for electrodynamic tether system, in: AIAA/AAS Astrodynamics Specialist Conference and Exhibit, Paper 2004-5313, Providence, Rhode Island, 2004.
[27] L. Jasper, Open-loop thrust profile development for tethered towing of large space objects (Ph.D. Dissertation), Aerospace Engineering Sciences Department, University of Colorado, Boulder, May 2014.
[28] M. Kim, C.D. Hall, Control of a rotating variable-length tethered system, Adv. Astronaut. Sci. 114 (2003) 1713–1732.
[29] P. Williams, Dynamic multibody modeling for tethered space elevators, Acta Astronaut. 65 (2009) 399–422.
[30] F.R. Driscoll, R.G. Lueck, M. Nahon, Development and validation of a lumped-mass dynamics model of a deep-sea rov system, Appl. Ocean Res. 22 (2007) 169–182.
[31] B. Buckham, M. Nahon, Dynamics simulation of low tension tethers, in: OCEANS'99 MTS/IEEE. Riding the Crest into the 21st Century, vol. 2, 1999, pp. 757–766.
[32] T.P. Dreyer, D.M. Murray, On the modeling of two-dimensional segmented representations of cable shape, Ocean Eng. 11 (1984) 609–625.
[33] A. Tustin, A method of analyzing the behavior of linear system in terms of time series, J. Inst. Electr. Eng. London 94 (1947) 130–142.